Available online at www.sciencedirect.com
SCIENCE DIRECT®
Journal of Nuclear Materials 352 (2006) 107–115
journal of nuclear materials
www.elsevier.com/locate/jnucmat

Study of carbon steel corrosion layer by X-ray diffraction and absorption methods

V. Malinovschi [a,*], C. Ducu [a], N. Aldea [b], M. Fulger [c]

[a] University of Pitesti, Research Center for Advanced Materials, Targul din Vale Street, No.1, 110040 Pitesti, Arges, Romania
[b] National Institutes for Research and Development for Isotopic and Molecular Technologies, P.O. Box 700, 3400 Cluj-Napoca, Romania
[c] Institutes for Nuclear Research, P.O. Box 0402, 0300 Pitesti, Romania

Abstract

To predict the behavior of structural metallic materials into the CANDU nuclear reactor, the oxide films on the surface were growth in a controlled manner using an autoclave simulating the environment specific to the nuclear reactor. In order to establish the structural changes of the oxide films, the X-ray diffraction (XRD), scanning electron microscopy (SEM), energy dispersive X-ray spectrometry (EDX) and extended X-ray absorption fine structure spectroscopy (EXAFS) analysis were used. Analysis performed showed differences in morphology of the oxide films from carbon steel samples exposed under different conditions corresponding to primary and secondary circuits in CANDU nuclear reactor. The oxide phases were identified and the thicknesses of the films were calculated. The agreement between results obtained by these methods was discussed according to the microstructure of the samples.

PACS: 28.41.Qb; 60; 80

1. Introduction

In nuclear reactors different types of metals and alloys are used as structural materials. In such environmental conditions these materials exposed to water results in corrosion. The prediction of corrosion behavior of the structural materials is very important from nuclear security and economical point of view. Carbon steel is widely used as pipe, mantle material and for the components of heat exchangers.

The evaluation and in depth understanding of nuclear materials behavior in an operating environment require utilization of surface analysis methods (XRD, SEM, EDX, EXAFS) and correlation of surface state of materials with their properties (mechanical, structural, corrosion resistance, etc.).

The characterization of the nuclear materials and of the material–environment interaction processes under operational conditions is related to the analysis of the non-homogeneous structures. Such complex analytical problem may be studied using complementary analytical techniques: XRD [1],

* Corresponding author. Tel.: +40 248 218804x234; fax: +40 248 216448.
E-mail address: malinov@electra.upit.ro (V. Malinovschi).

0022-3115/$ - see front matter © 2006 Elsevier B.V. All rights reserved.
doi:10.1016/j.jnucmat.2006.02.044

SEM and EDX [2], EXAFS [3], and specific data processing methods.

XRD methods can yield microstructure information: qualitative and quantitative phase analysis; determination of grain alignment (texture) in polycrystalline materials; determination of microstructural properties (i.e., mean crystallites diameter, mean square microstrain, size distribution, etc.); determination of the thickness of oxide films, in some cases; determination of crystallographic phases from oxide films by low angle incidence diffraction, etc. By XRD the minimum thickness of oxide films on carbon steel that can be investigated is tens of nanometers and the maximum thickness of some micrometers.

SEM and EDX are adequate techniques for determining grain morphology and elemental composition (qualitative and quantitative). EDX can yield information about elemental composition from some micrometers depth.

The study of extended X-ray absorption fine structure can yield structural information about the local environment around a specific atomic constituent in the investigated materials.

The complementarities of XRD and EDX are given by phase analysis. Mean crystallites diameter determined by XRD can be correlated with grain size determined by SEM analyses. The single phase composition of oxide films on carbon steel (Fe_3O_4) determined by XRD can be correlated with modification of coordination number for iron determined by EXAFS measurements.

The characterization of the thin films developed in the operating conditions in CANDU systems on carbon steel was investigated.

2. Experimental

The composition (in wt%) of the studied carbon steel was: Fe–98.66, Mn–1.00, Al–0.06, Ni–0.018, Cr–0.01, C–0.19, Si–0.037, P–0.021, S–0.004.

Table 1
Parallelepiped samples of carbon steel SA 516 by autoclaved generalized corrosion test

No.	Code	Environment	Water (pH, T, P)	Time of exposure (d)
1	S1	Secondary	pH = 9.7	80
2	S2	circuit	$T = 533$ K	180
			$P = 5.1$ MPa	
3	S3	Primary	pH = 10.5	64
4	S4	circuit	$T = 583$ K	130
			$P = 10$ MPa	
5	Reference	–	–	–

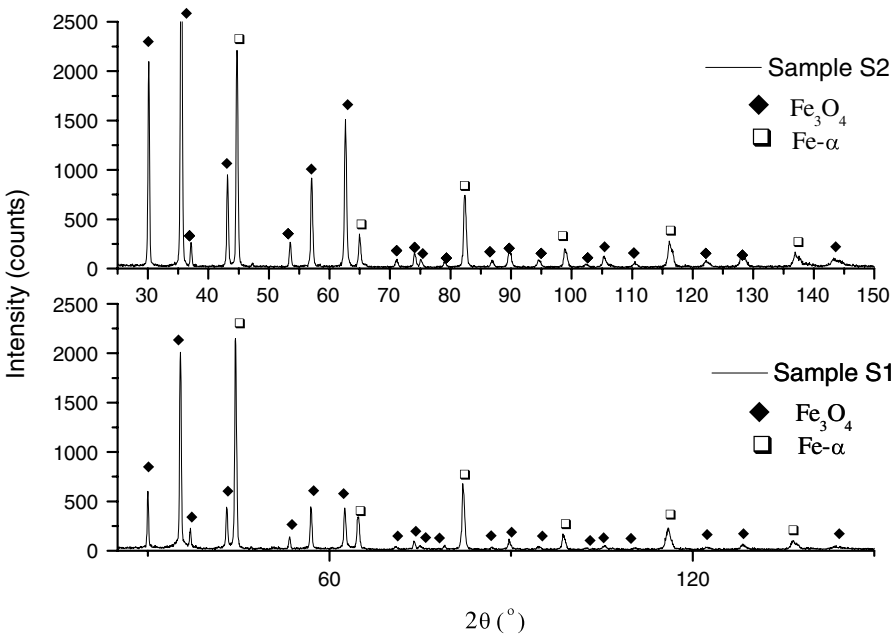

Fig. 1. The XRD pattern for S1 and S2 samples (secondary circuit conditions).

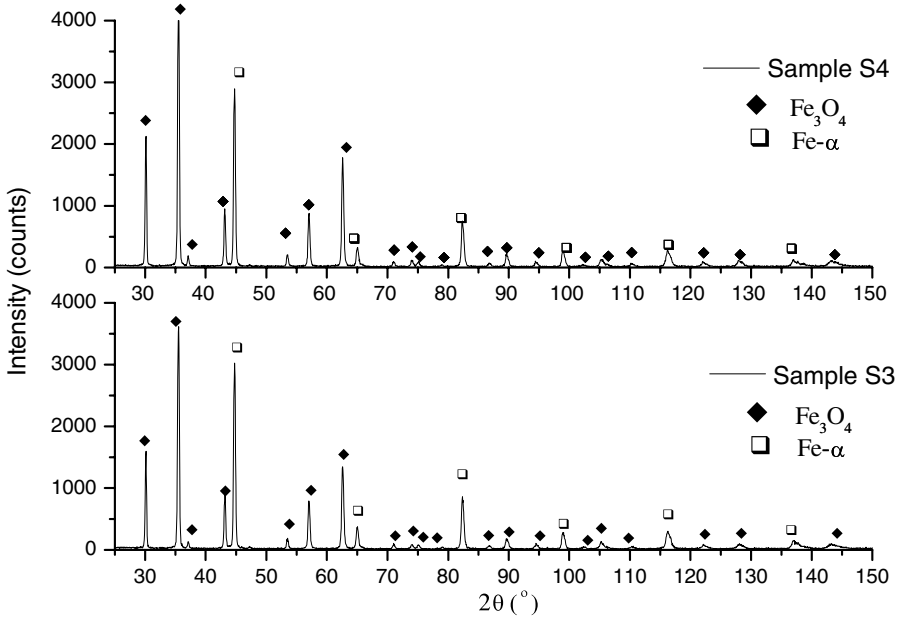

Fig. 2. The XRD pattern for S3 and S4 samples (primary circuit conditions).

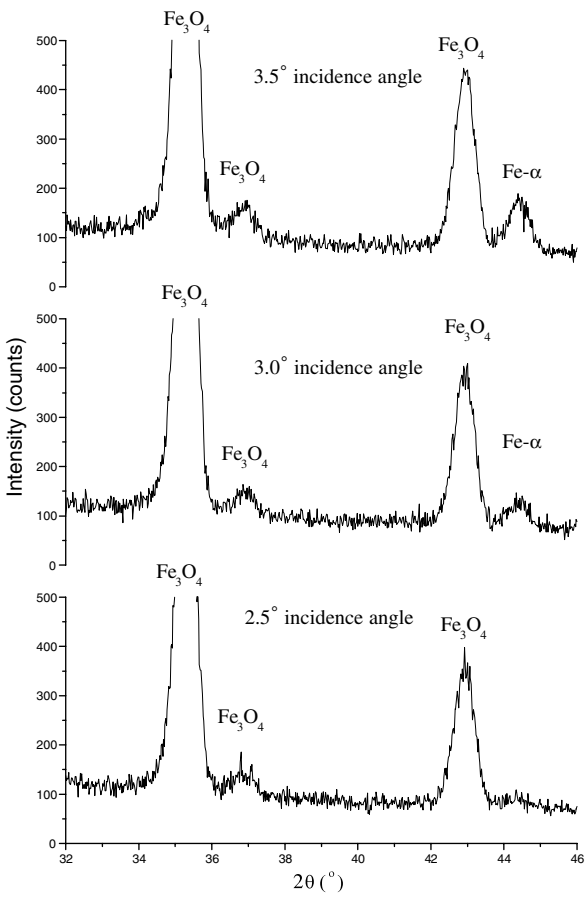

Fig. 3. Low angle incidence XRD pattern for sample S1.

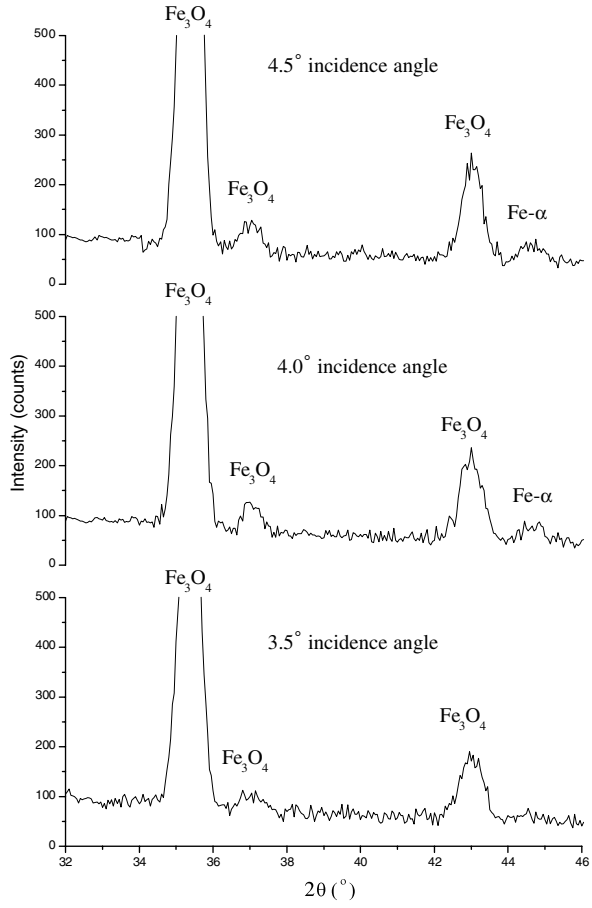

Fig. 4. Low angle incidence XRD pattern for sample S2.

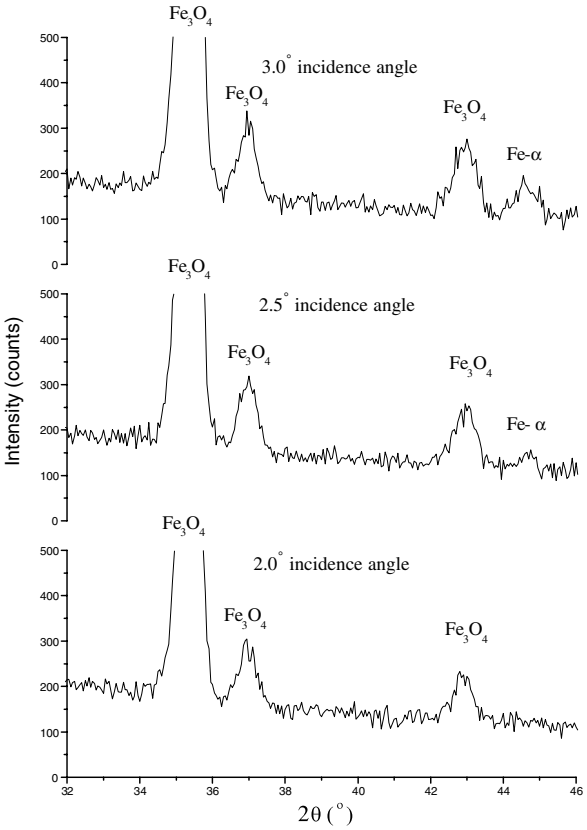

Fig. 5. Low angle incidence XRD pattern for sample S3.

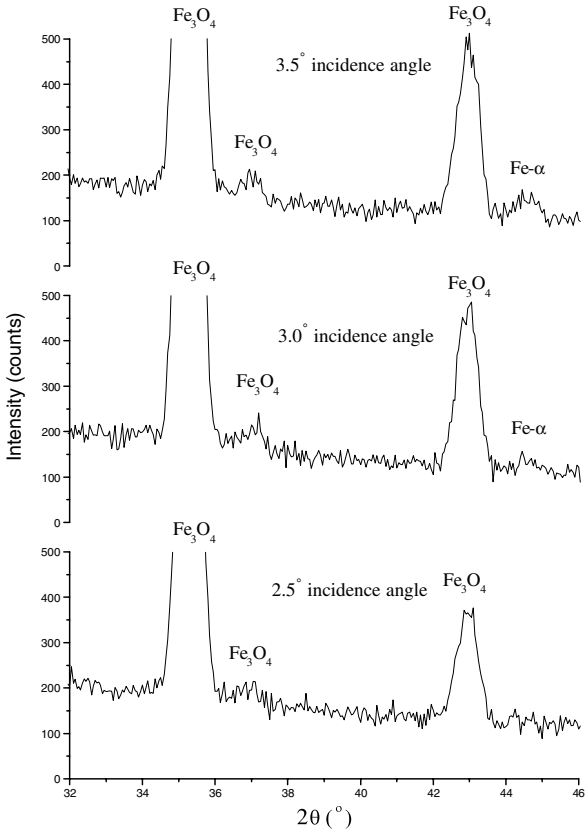

Fig. 6. Low angle incidence XRD pattern for sample S4.

2.1. Test conditions

The generalized corrosion tests were performed in solutions, which simulate the environment specific to the primary and, secondary circuits of CANDU nuclear reactor [4,5].

For primary environment circuit demineralized water (H_2O) solutions with pH 10.5, regulated with LiOH, was used. The tests were performed at a temperature of 583 K and a pressure of 10 MPa.

For secondary environment circuit, demineralized water solutions with volatile amine and hydrazine for regulating pH at 9.7 were used. The test conditions were: temperature 533 K and pressure 5.1 MPa. The tests were performed in PROLABO static autoclaves. The solutions conductivity used in chemical and electrochemical tests as well as the pH was measured with a CONSORT C835 multiparametric tester.

Before autoclaving the samples were prepared by mechanical and electrochemical polishing, cleaning in organic solvents and drying at 373 K for 5 min. The area of surface and the mass of the samples were quantified.

Table 1 presents the samples analyzed, codes of samples, time of exposure and water parameters (pH, T, P).

2.2. XRD measurements

The X-ray diffraction data of carbon steel SA 516 oxide films and etalon sample of carbon steel SA 516 were collected at room temperature. Data acquisitions were made with a DRON UM1 diffractometer connected with PC. A horizontal powder goniometer in Bragg–Brentano focusing geometry with graphite monochromator was used. The incident Cu-K_α line, $\lambda = 1.54178$ Å, at 35 kV and 30 mA was used. The typical experimental conditions were: 3 s for each step, range angle $2\theta = 20$–150°, with a step of 0.05°. The patterns obtained in these conditions were used to make qualitative phase analysis [6]. The range angle $2\theta = 32$–46°

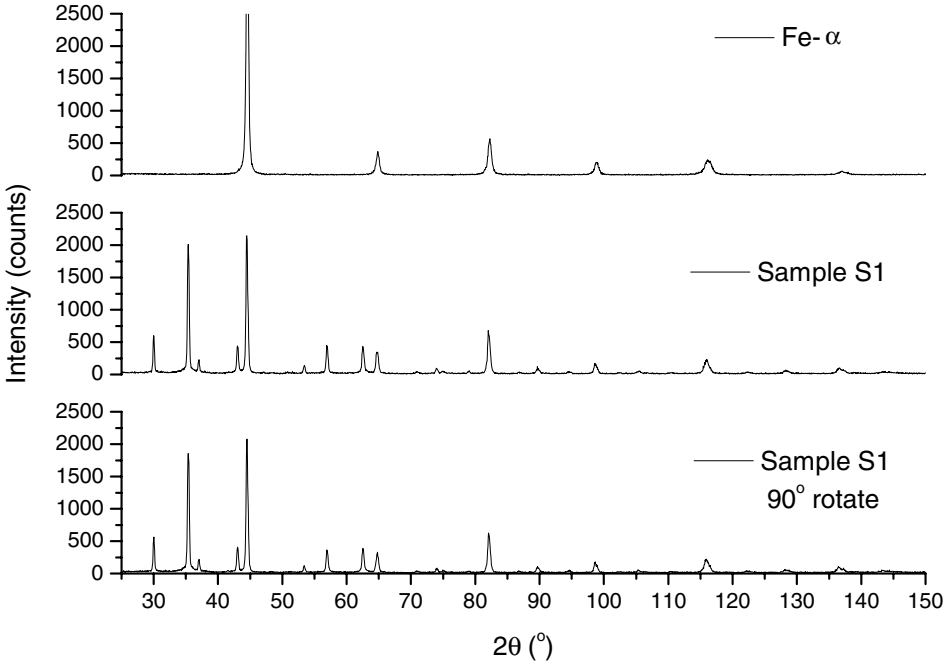

Fig. 7. The XRD pattern for reference and S1 at two different sample positions.

containing the 100% intensity peaks of Fe_3O_4 ($2\theta = 35.47°$), Fe_2O_3–hematite ($2\theta = 33.19°$), and Fe-α ($2\theta = 44.71°$) were measured with a better statistics, 10 s for each step with a step of 0.02°. In the same angular range the low angle incidence diffraction in order to determine the phase's presence in the surface films, from 2.0° to 4.5° incidence angle was performed.

2.2.1. EXAFS measurements

The transmission EXAFS measurements were carried out of the 4W1B beam lines in the Beijing Synchrotron Radiations Facilities (BSRF), which was operating at room temperature [7].

The 4W1B beam line is an unfocused monochromatic X-ray beam with 4 mrad of horizontal acceptance. The X-rays are monochromatised by a fixed exit Si double crystal monochromator. The features of the 4W1B beam line are: an energy range of 3.5–22 keV; an energy resolution of $\Delta E = 1$–3 eV at $E = 10$ keV and a Bragg angle range of 5–70°. Crystals Si(1 1 1), Si(2 2 0) and Si(3 1 1) can be alternatively used as monochromator. A Fe_2O_3 and Fe_3O_4 pure powders, and, a Fe-α foil were used as standard samples. The absorption coefficients of the standard samples edge were determined using a Si(1 1 1) double-crystal monochromator. The X-ray intensities of the incident and transmitted beams were recorded using ionization chambers. Harmonics were rejected by detuning of the monochromator. The whole experimental system was controlled by personal computer PS/2 for automatic data acquisition. Special care was taken in the sample preparation, especially with regard to the thickness and homogeneity

Table 2
Microstructural parameters of oxide films calculated from X-ray diffraction patterns

Sample	Thickness by XRD (μm)	Thickness by gravimetry (μm)	Mean crystallites size (nm)	Mean square microstrain (%)
S1	0.58	0.68	146 ± 45	0.103 ± 0.015
S2	1.36	1.39	Peak broadening contributed by crystallite size is negligible	0.174 ± 0.080
S3	1.16	1.21	75 ± 29	0.195 ± 0.090
S4	1.37	1.45	Peak broadening contributed by crystallite size is negligible	0.177 ± 0.056

of samples, to obtain absorption spectra of good quality. For autoclaved samples we worked in the fluorescence setup arrangement. We used an energy range from 7000 to 8000 eV for the measurement of the absorption coefficients.

The EXAFS analyses of the absorption coefficient were processed using the computer code CDXAS [8].

2.3. SEM and EDX measurements

Scanning electron microscopy measurements were performed with an electronic microscope JEOL-JSM 5600 LV. The surfaces of the samples were analyzed by image acquisition and by energy dispersive X-ray spectrometry (EDX).

3. Results and discussion

3.1. XRD results

Figs. 1 and 2 show the XRD pattern for investigated samples. The phase analysis reveals only two crystallographic phases in these samples: Fe-α (cI2/1, bcc) and Fe_3O_4 (magnetite, cub. cF56/2).

Low angle incidence diffraction analysis was applied for finding the distribution of these phases in the oxide films. The incident angle varied between 2.0° and 4.5°. These patterns were acquisitioned with a good statistics for the possible Fe_2O_3–hematite (33.19°) identification in the oxide films. The Fe_2O_3–hematite (33.19°) will not appear even in secondary or primary circuits. In Figs. 3–6 we show the low angle incidence diffraction patterns for sample S1, S2, S3 and S4, respectively. From the analysis of these patterns, we observe that the Fe_3O_4–magnetite is the only phase in the thin films on the surface. The different incidence limit angle at which the Fe-α phase appears is due to the different thickness of the films.

In Fig. 7 are shown the diffraction patterns of reference sample and S1 acquisitioned in the angular range $2\theta = 25$–150° at two sample positions. The second position was obtained by sample rotate with 90° around normal at sample surface. These patterns are identical which means that the oxide films are not textured.

Thickness of oxide films was evaluated by X-ray diffraction patterns as follows:

(a) From the diffraction pattern of reference sample (Fig. 7) were calculated integral intensity of (1 0 1) Fe-α line (I_{ref}). The penetration depth d of radiation in standard sample was calculated using the relation given in Ref. [1], p. 369:

$$t \geqslant \frac{3.2}{\mu}\frac{\rho}{\rho'}\sin\theta. \quad (1)$$

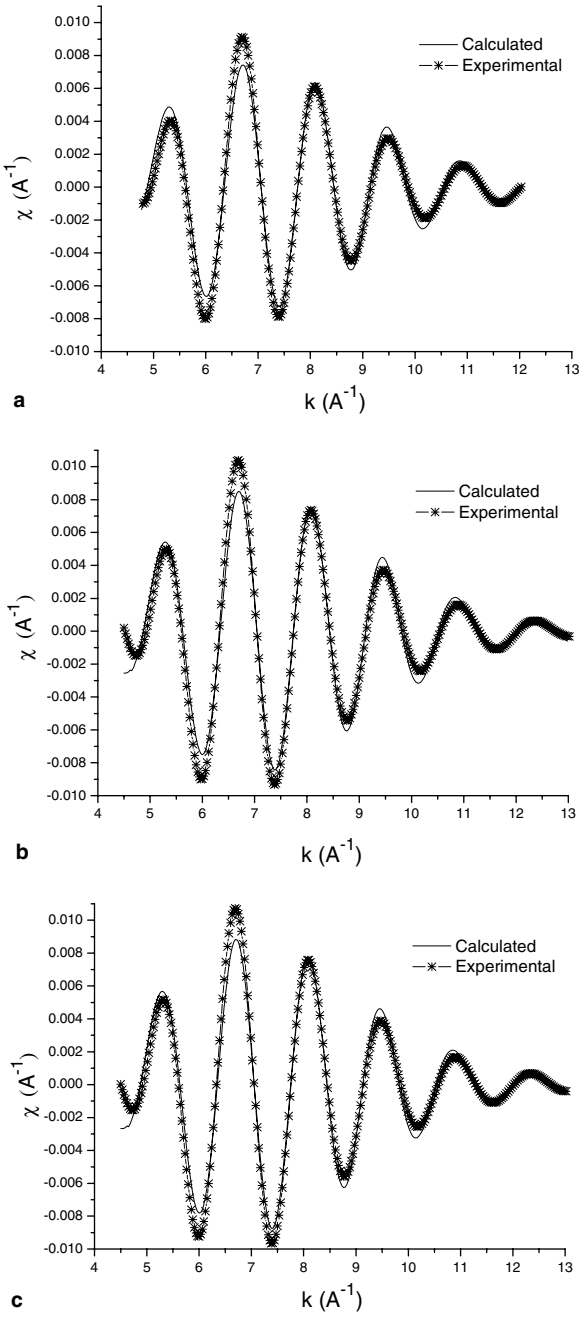

Fig. 8. The experimental and calculated EXAFS signals of the first shell for S2 (a), S3 (b) and S4 (c).

Table 3
Coordination number and first shell radius obtained by EXAFS measurements

Sample	N (number of atoms)	R Shell radius (nm)
Fe-α reference	8.00	0.248
S2	5.12	0.249
S3	4.97	0.249
S4	5.36	0.250

From the relation

$$d_{\mathrm{ref}} = \frac{3.2}{\mu_{\mathrm{Cu}}(\mathrm{Fe}\alpha)} \sin\theta. \tag{2}$$

the penetration depth of the Cu K_α line in Fe-α obtained is calculated to be $d_{\mathrm{ref}} \cong 4.77\ \mu\mathrm{m}$.

(b) From the diffraction patterns of S1–S4 samples (Figs. 1 and 2) were calculated integral intensities of (1 0 1) Fe-α line ($I_{\mathrm{Fe}\alpha}$) and (1 1 3) Fe_3O_4 line ($I_{\mathrm{Fe_3O_4}}$).

(c) The thickness of Fe-α ($d_{\mathrm{Fe}\alpha}$) from S1–S4 that contribute at diffraction pattern of Fe-α is calculated by relation

$$\frac{d_{\mathrm{ref}}}{d_{\mathrm{Fe}\alpha}} = \frac{I_{\mathrm{ref}}}{I_{\mathrm{Fe}\alpha}}. \tag{3}$$

(d) The Fe_3O_4 film thickness of S1–S4 samples that contribute at diffraction pattern of Fe_3O_4 is calculated by relation

$$\frac{d_{\mathrm{Fe_3O_4}}}{d_{\mathrm{Fe}\alpha}} = \frac{I_{\mathrm{Fe_3O_4}}}{I_{\mathrm{Fe}\alpha}} \frac{\mu_{\mathrm{Cu}}(\mathrm{Fe_3O_4})}{\mu_{\mathrm{Cu}}(\mathrm{Fe}\alpha)} \frac{\sin\theta_{(1\,1\,3)}}{\sin\theta_{(1\,0\,1)}}. \tag{4}$$

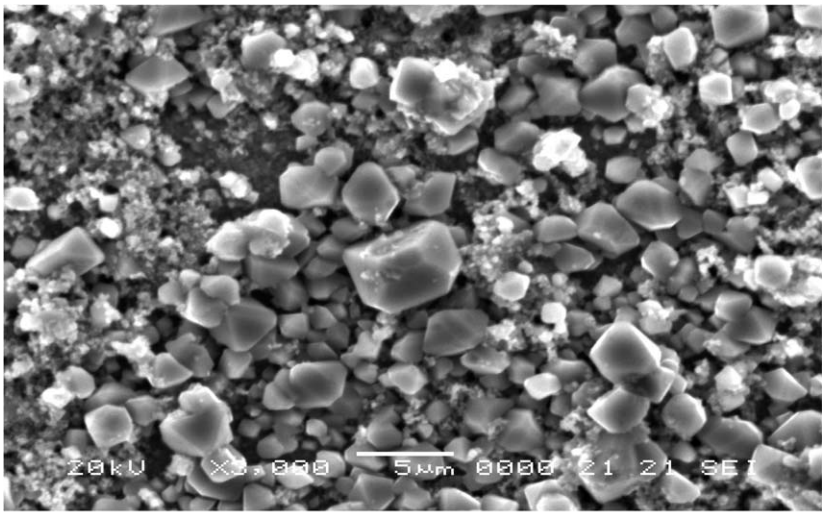

a

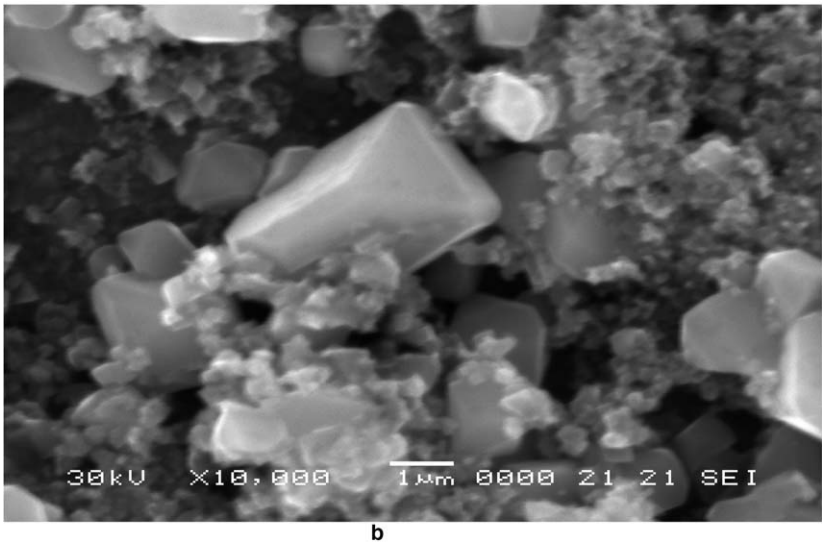

b

Fig. 9. The SEM image of sample S2.

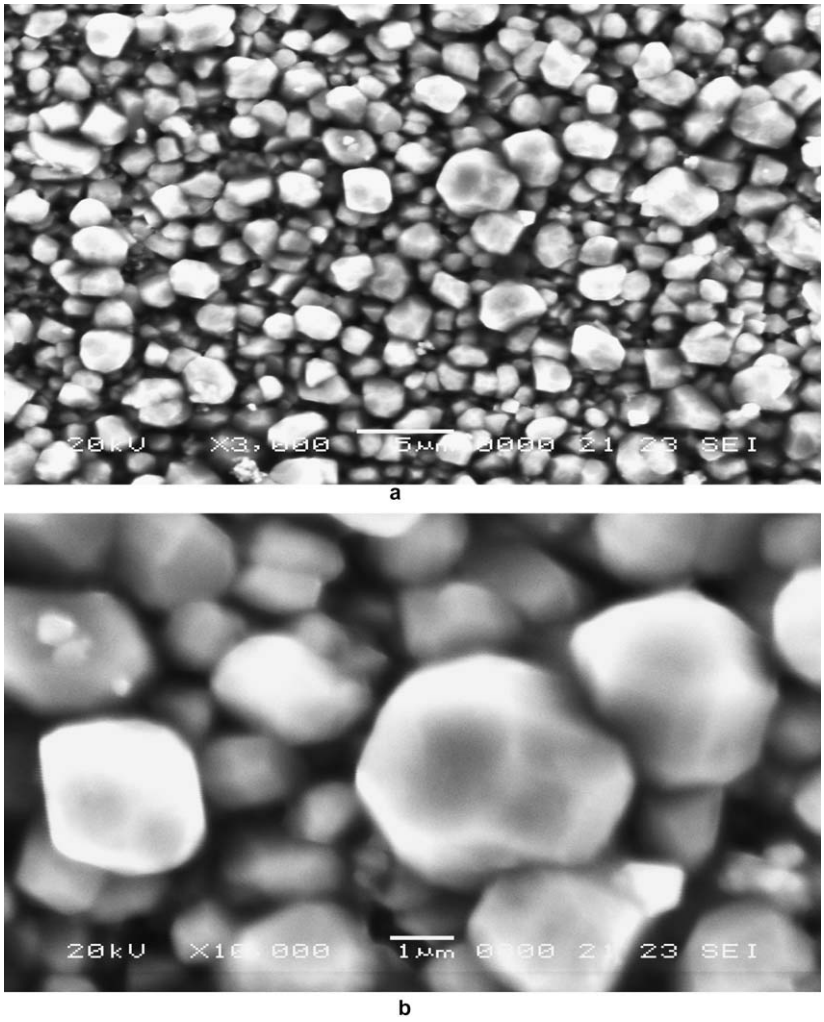

Fig. 10. The SEM image of sample S4.

Numerical results obtained by this model are presented in Table 2 and compared with the values of thickness determined by gravimetric analyzes.

Mean crystallites size $\langle D\rangle$ and mean square microstrain $\varepsilon_0 = \sqrt{\langle \varepsilon^2\rangle}$ for Fe_3O_4 phase of S1–S4 samples were calculated from the singlet physical line diffraction width of (113) and (226). The line width Δq ($q = \frac{4\pi}{\lambda}\sin\theta$ module of the diffraction vector) depends by the $\Delta\theta$ by relation: $\Delta q = \frac{1}{\lambda}\cdot\frac{\pi^2}{90}\cdot\cos\theta\cdot\Delta\theta$. Considering that integral width of grain profile in q space (b_L) is described by a first order Lorentz function ($n = 1$) and integral width of strain profile in q space (b_G) is described by a Gauss function. From hypothesis of spherical grains (confirmed by texture absence) mean crystallites diameter is calculated with relation: $\langle D\rangle = \frac{8}{3}\cdot\frac{\pi}{b_L}$ and mean square microstrain is calculated with relation: $\varepsilon_0 = (2\pi)^{-3/2}\cdot d^{(1)}_{hkl}\cdot b^{(1)}_G$ where $d^{(1)}_{hkl}$ is interplanar distance for first reflection order. The quantities b_G and b_L are determined from the equations system:

$$B_1 = \frac{2}{3}\cdot b_L + \sqrt{\left(\frac{b_L}{3}\right)^2 + b_G^2} \tag{5}$$

$$B_2 = \frac{2}{3}\cdot b_L + \sqrt{\left(\frac{b_L}{3}\right)^2 + 4b_G^2} \tag{6}$$

where B_1 and B_2 are integral width of physical singlet for first and second reflection order, respectively.

The numerical results obtained by this model are presented in Table 2.

3.2. EXAFS results

Fig. 8 shows the fitting experimental results of EXAFS pattern of S2, S3 and S4 samples, for the first coordination shell with the calculated values. The extraction of the EXAFS signal is based on the edge energy E_0 determination, followed by background removal by pre-edge and after-edge baseline fitting with different possible modeling functions. Based on [9], ($n = 1$, a Kaiser window), the Fourier transforms of the radial structure function for the first shell are obtained. Coordination numbers and first shell radius obtained for S2, S3 and S4 samples are presented in Table 3.

The values of the first coordination shell radius are similar for all samples. The lower values of coordination numbers are due to the presence of Fe_3O_4.

3.3. SEM and EDX results

In Figs. 9 and 10 are presented the surface images of samples S2 and S4. The quantitative analysis of the EDX pattern for surface of S2 sample confirm Fe = 68.99 wt% and O = 31.01 wt%. By image analyses the grain size of Fe_3O_4 were observed to be greater and much homogeneous in primary circuits (mean size is greater than 1 μm) than in secondary circuits.

4. Conclusions

A study of corrosion oxide films grown on the surface of carbon steel in environmental conditions specific to primary and secondary circuits in CANDU nuclear reactor has been conducted. The aim of this study was to produce data on the microstructure of surface films.

- From low angle incidence X-ray diffraction measurements, we found that our oxide films have only Fe_3O_4–magnetite phase.
- Weight concentration of iron from Fe_3O_4 oxide film determined by XRD (72%) is in good agreement with weight concentration determined by EDX (69%).
- The thickness of oxide films calculated by XRD are in good agreement with gravimetric analysis results.
- The mean crystallite sizes, for a given time of exposure, calculated from the XRD spectra are in good agreement with the grain sizes determined by SEM.
- Decrease in of coordination numbers of Fe calculated by EXAFS is due to Fe_3O_4–magnetite presence determined by XRD.

References

[1] H.P. Klug, L.E. Alexander, X-ray Diffraction Procedures for Polycrystalline and Amorphous Materials, second ed., Wiley, New York, 1974.
[2] P.E.J. Flewit, Physical Methods for Materials Characterization, Institute of Physics, Publishing Ltd., London, 1994.
[3] E.A. Stern, in: D.C. Koningsberger, K. Prins (Eds.), Theory of EXAFS, X-ray Absorption: Principles, Applications, Techniques of EXAFS, SEXAFS and XANES, Wiley, New York, 1988.
[4] M. Fulger, Contribution at degradation kinetics of some alloys used in NPP, PhD thesis, University of Bucharest, 2004.
[5] R. Baboian, Corrosion Tests and Standards: Application and Interpretation, ASTM Manual, vol. 1, 1995.
[6] C. Ducu, V. Malinovschi, I. Iosub, Rev. Chimie 54 (8) (2003) 666.
[7] N. Aldea, A. Gluhoi, P. Marginean, C. Cosma, Xie Yaning, Spectrochim. Acta A, B 455 (2000) 997.
[8] A. San-Miguel, Phys. B 208&209 (1995) 177.
[9] E.A. Stern, Phys. Rev. B 10 (1974) 3027.